Multilayered Center-of-Pressure Sensors for Robot Fingertips and Adaptive Feedback Control

Yosuke Suzuki, *Member, IEEE*

***Abstract*—This letter proposes a sheet-shaped force sensor for covering a robot fingertip. The sensor consists of flexible materials and can be adaptively designed to the shape of the fingertip. When a load acts on the sensor, the contact position and both normal and tangential forces can be detected. Experimental results show the sensor characteristics as follows: The contact position can be estimated in high accuracy if it is enough separated from the boundary of the sensing area, the normal force up to 4 N can be estimated independent with the contact position, and the tangential force can be estimated by calibration while the sensitivity remains to be improved. This letter also presents two feedback control laws of a robot finger mounted with the proposed sensor. One is to keep both a contact position and normal force at constant to a target object, and the other is to keep rolling contact even if the object moves while touching. The availability of the control laws are confirmed through motion experiments.**

***Index Terms*—Feedback control, robotic hand, tactile sensor.**

I. Introduction

FORCE sensation is one of the most important abilities in human tasks. It enables them to dexterously handle objects even if there are uncertainties and variations in the conditions or the environments. Demand for automation of complicated tasks is increasing especially in material handling. Robot manipulators had originally executed tasks relying on the repeatability of the position. However, based on the above demand, many researches have been addressed for adding flexibility to the robots in two general methodologies; mechanical compliance by embedding elastic parts, and active compliance control based on force sensing. Imitating the manner of humans, both methodologies would be essential for dexterous manipulation.

Mechanical compliance contributes to progress of success rates of tasks in uncertainties. One of the most widely used mechanisms is a remote center compliance device [1]. In the field of robotic hands, researchers have proposed various designs using mechanical compliance [2]–[4]. Joint compliance is adopted in a number of works. For example SDM Hand has a tendon driven mechanism with flexure joints and stiff links [5]. On the other hand, jamming grippers and fluid fingertips are examples arranging compliance at the links which directly contact with target objects [6]–[8]. The benefit of the mechanical compliance is large; (i) robustness on position error to target objects, (ii) easiness of contact force control in an intended range, (iii) avoidance of impact force on both objects and fingertips, and (iv) execution of enveloping grasp owing to large deformation. However, the mechanisms have disadvantages in reliability and stiffness in principle.

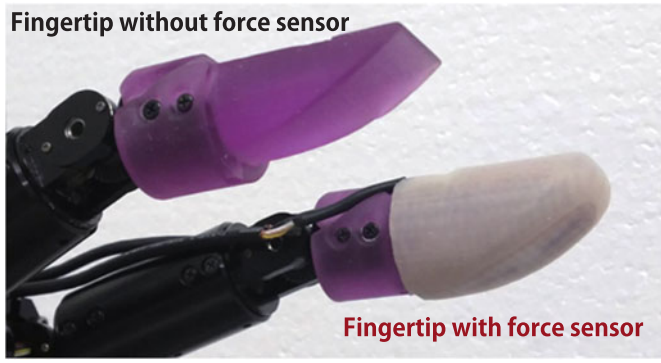

Fig. 1. Overview of fingertips with and without the proposed force sensor.

Active compliance control realizes equivalent property as containing elastic parts, by the use of force sensing [9], [10]. For instance Raibert *et al.* proposed a hybrid control law of a manipulator based on force sensing at the wrist [11]. One problem of such control is the requirement for mounting force sensors, which should not interfere the movement of the robots or decease the performance of the robots such as payload and durability. To improve this problem, force sensorless control strategies have been proposed [12]–[14]. The strategies estimate the reaction force from the joint torques of the robots. These are widely adopted in recent manufacturing robots. However, the estimation requires precise models of the robots, and thus, it is difficult if there are unignorable frictional losses, backlashes, and mechanical compliances in the robot mechanisms.

From the above points of view, it is valuable to mount force sensors with less-invasive designs on robot fingertips, which directly contact with manipulation targets. This letter proposes a sheet-shaped flexible force sensor for a robot fingertip as shown in Fig. 1. The sensor consists of a flexible substrate, pressure-conductive rubbers and a soft cover sheet. The shape can be customized to fit various fingertip shapes and overlay the whole surface. When a load acts on the fingertip, the center position of the pressure distribution and both normal and tangential forces are detected.

Manuscript received February 15, 2017; accepted June 13, 2017. Date of publication July 4, 2017; date of current version July 19, 2017. This letter was recommended for publication by Associate Editor J. McInroy and Editor Prof. J. Wen upon evaluation of the reviewers' comments. (*Corresponding author: Yosuke Suzuki*.)

The author is with the Faculty of Mechanical Engineering, Institute of Science and Engineering, Kanazawa University, Kanazawa 920-1192, Japan (e-mail: suzuki@se.kanazawa-u.ac.jp).

Digital Object Identifier 10.1109/LRA.2017.2723469

Tactile sensing is helpful with providing action-related information, control parameters in manipulation, and estimation of contact parameters [15]. There are various types of sensing methods utilizing resistive [16]–[18], capacitive [19], optical [20], magnetic [22], piezoelectric [23], and so on. One of the most related works is a Center of Pressure (CoP) sensor by Shimojo *et al.*, which uses a pressure conductive rubber as detector and quickly calculates the center position of the pressure distribution by analog computation [16], [17]. The sensor proposed in this letter applies a multi-layered structure of the CoP sensors for detecting tangential force. BioTac is a sensor-embedded fingertip, which utilizes conductive fluid for detecting pressure distribution [18]. A force sensor by OptoForce mounts light emitter and receivers in a deformable void, and estimates the force from the reflection in the void [20]. Vogt *et al.* proposed a soft multi-axis force sensor composed of a molded elastomer and liquid metal in a flow channel formed inside the elastomer [21]. Tomo *et al.* developed a distributed 3-axis force sensor by measuring the displacement of magnets embedded in soft materials with Hall effect sensors [22]. Yu *et al.* proposed flexible and responsive 3-axis force sensor using a PVDF film and a PDMS layer with bumps [23]. In general, detection of tangential force requires thickness of the sensor because a flexure element needs to be large in the thickness direction. However, it brings restrictions in fingertip design.

The features of the proposed sensor are as follows:

1) Thin and flexible
2) Adaptive design to various fingertip shapes
3) Quick detection of a contact position and both normal and tangential forces.

There are requirements for the sensor mounted on a robot: the sensor less restricts the design of the robot in such as shape, volume, weight, power supply and wiring, and it provides useful information for the mechanism and the motion of the robot. From this viewpoint, the richness of the amount of information is not necessarily required. Matching between the acquired information and the target task is important. Particularly, since mechanical interaction with objects occurs during the operation of the tactile sensor, a high-speed response is desirable to prevent grasping errors. This is not just a problem of the sampling rate but also the usability for the motion planning of the robot from the obtained information. The proposed sensor provides not rich but useful information for estimating the movement of the contacting object without complicated processing. That is, this sensor cannot detect distribution of pressure on the fingertip, but it can determine the center position and the total force of the pressure distribution, which enables highly-responsive tactile servoing of the fingertip. The shape and size of the sensitive area can be designed according to the predetermined contour of the fingertip with light weight and reduced wiring. These properties are suitable for managing the contact state to the moving object by a full-actuated robotic hand with real-time control. The design method and the sensing ability are shown in the Sections II and III. In the Section IV, the availability of the sensor for realizing adaptive feedback controls of the robot finger by motion experiments.

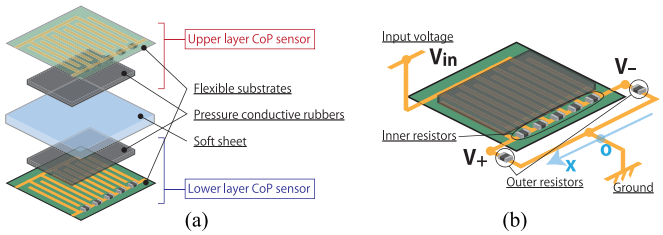

Fig. 2. Structure of the proposed sensor ((a) compositional elements: a soft sheet and two layers of CoP sensors each of which is composed of a flexible substrate and a pressure conductive rubber, (b) circuit diagram of CoP sensor).

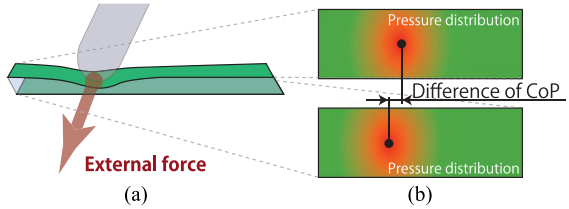

Fig. 3. Principle of tangential force sensing ((a) example of loading condition where both normal and tangential forces act on the sensor, (b) difference of pressure distribution and CoP between the two layers).

II. Sensor Structure

A. Sensing Principle

The structure of the proposed sensor is shown in Fig. 2. Two layers of identical CoP sensors are arranged so as to sandwich a soft material sheet. Each CoP sensor consists of a pressure conductive rubber sheet and a flexible substrate. The substrate contains comb-shaped electrodes and an analog computing circuit using resistors called inner/outer resisters. The electrodes are for detecting resistance change of the rubber by pressure, and the circuit is for calculating both the center position x_c and the total amount I_{all} of the current flowing through rubber. These values can be derived from the two voltages in the circuit V_+ and V_- by the following equations,

$$x_c = \left(1 + \frac{R_0}{r}\frac{2}{N-1}\right)\left(\frac{V_+ - V_-}{V_+ + V_-}\right) \tag{1}$$

$$I_{all} = \frac{V_+ - V_-}{R_0} \tag{2}$$

Here, R_0 and r are the resistances of the outer and inner resistors, and N is the division number of the comb-shaped electrodes. x_c is a normalized in $[-1, +1]$.

When the two CoP sensors are arranged in parallel layers, the pairs of x_c and I_{all} indicate the difference of normal force distributions between the two layers. Since the sensor structure has flexibility, deformation easily occurs according to external force as shown in Fig. 3. Therefore, s_x, which is defined as the difference of x_c as the following equation, reacts to tangential force acting on the sensor.

$$s_x = x_{c-i} - x_{c-o} \tag{3}$$

Here, the suffixes i means the inside layer and o means the outside layer.

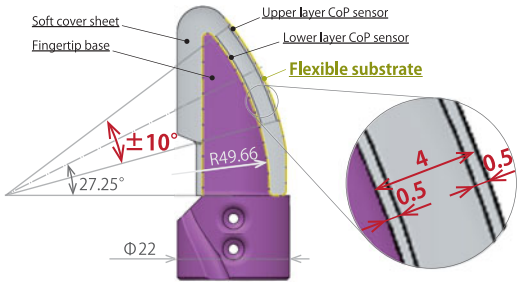

Fig. 4. Sectional view of a sensor designed for a robot fingertip.

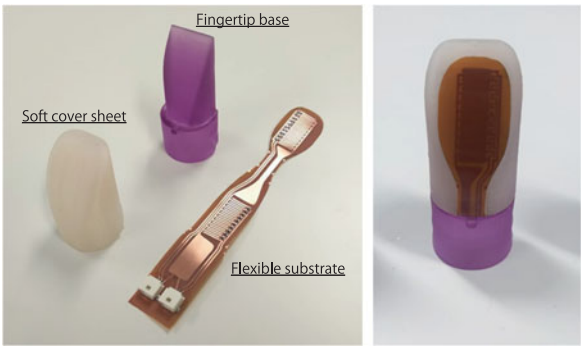

(a) (b)

Fig. 5. Overviews of the compositional elements (a) and an assembled fingertip (b).

In summary, the contact position can be estimated from x_{c-i} or x_{c-o}, the normal force from I_{all-i} or I_{all-o}, and the tangential force from s_x, respectively.

B. Design for Robot Fingertip

Fig. 4 is a sectional view of a sensor designed for a robot fingertip. The thickness of each CoP sensor is 0.5 mm. Considering about the soft cover sheet between the two CoP sensors, it is preferable to be thick and deformable for sensing tangential force, while the interference to the original fingertip shape should be small. Thus, the interval between the CoP sensors is determined as 3 mm, and so the thickness of the whole sensor is 4 mm. The soft cover sheet can be molded with rubber-like resin (shore A hardness: 20) by using a 3-D printer (ARM10, Roland DG Corp.). The sensing area spreads in the range of ± 10 deg along the curved surface (the length is approximately 18 mm,) and the width is 6 mm.

Fig. 5 shows (a) the composition elements and (b) the assembled fingertip. In order to protect the sensor surface, a 1 mm cover sheet made of the rubber-like resin is attached on it. The parameters of the CoP sensors are as follows: $R_0 = 2$ kΩ, $r = 100\ \Omega$ and $N = 11$. Note that this model adopts 1-D CoP sensors for ease of fabrication. A design using 2-D CoP sensors is also feasible although it requires complicated arrangement of electrodes and wires. Hereafter, we call the sensor as "fingertip sensor."

III. Experiments on Sensor Characteristics

This section describes four experiments to examine the following characteristics of the fingertip sensor.

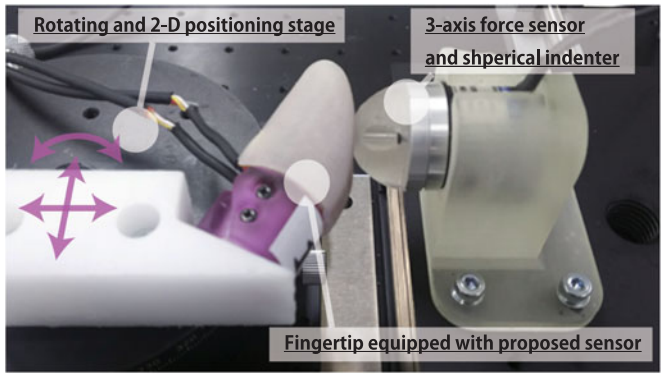

Fig. 6. Overview of the experimental setup.

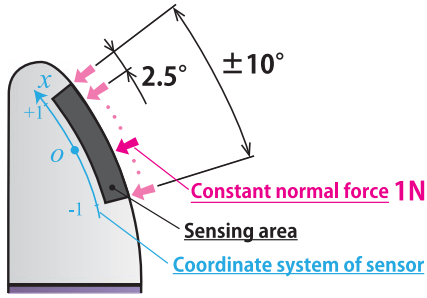

Fig. 7. Loading condition of the experiment to examine contact position detection.

1) Contact position detection based on x_{c-i} and x_{c-o}
2) Normal force detection based on I_{all-i} and I_{all-o}
3) Tangential force detection based on $s_x (= x_{c-i} - x_{c-0})$
4) Hysteresis, repeatability, responsiveness and durability.

A. Experimental Method

The overview of the experimental setup is shown in Fig. 6. The fingertip equipped with the sensor is fixed on a rotating and 2-D positioning stage. A spherical indenter is fixed on a 3-axis force sensor (USLG25, measuring range XY: ± 5 N and Z: $+10$ N, Tec Gihan Co., Ltd.). Compression at an arbitrary point is executed by moving the stage, with changing the normal force and the tangential force. Comparing the outputs of the fingertip sensor and the 3-axis force sensor, we examine the characteristics in each loading condition. Note that viscoelasticity of the soft materials of the fingertip sensor brings creep property. In order to suppress the effect, we measure the data at the time approximately 60 seconds after each compression. However, it is difficult to precisely control the loading force at a target value.

B. Contact Position Detection Based on x_{c-i} and x_{c-o}

To confirm whether a contact position can be estimated from x_{c-i} or x_{c-o}, compression is executed at different points in the normal direction with a constant force. The loading condition is shown in Fig. 7. The rotational pitch of the compressed points is 2.5 deg among the sensing area ± 10 deg. The normal force is nearly constant at 1 N in each of the compression points.

Fig. 8(a) shows the detected values of x_{c-i} and x_{c-o} to the theoretical values of x_c calculated from the angle of the compression points. It can be seen that both x_{c-i} and x_{c-o} linearly

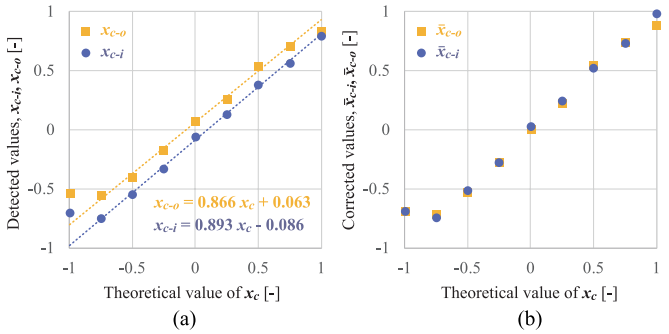

Fig. 8. Experimental result of contact position detection ((a) relationship between the detected values x_{c-i}, x_{c-o} and the theoretical values of x_c, (b) relationship between the corrected values $\bar{x}_{c-i}$, $\bar{x}_{c-o}$ and the theoretical values of x_c).

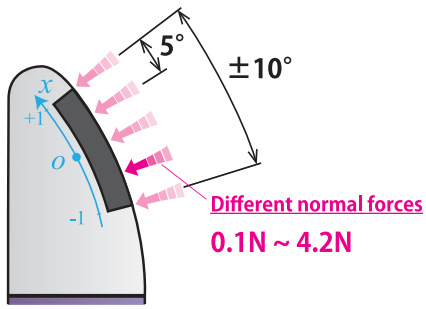

Fig. 9. Loading condition of the experiment of normal force detection.

change according to the theoretical values with small errors. The errors are thought to be caused by fabrication error of the sensor. The linearity is especially high, if omitting the data at the compression points ±10 deg where are the boundaries of the sensing area. So, approximate lines derived from the data of $-7.5 \sim +7.5$ deg are added in the graph. By using the coefficients of the approximate lines, the following correction equations are obtained.

$$\bar{x}_{c-i} = 1.120 x_{c-i} + 0.086, \tag{4}$$

$$\bar{x}_{c-o} = 1.154 x_{c-o} - 0.063. \tag{5}$$

Here, $\bar{x}_{c-i}$ and $\bar{x}_{c-o}$ are the corrected values of x_{c-i} and x_{c-o}.

Fig. 8(b) shows the same graph of the corrected values $\bar{x}_{c-i}$ and $\bar{x}_{c-o}$. The corrected values of both layers are enough close to the theoretical values in the range of $-0.75 < x_c < 0.75$. Converting to the position error on the fingertip surface, the maximum error is 0.29 mm at the inner layer and 0.50 mm at the outer layer. Note that these values depend on the loading condition such as the shape of the indenter. Under the condition of this experiment, the contact position can be estimated in high accuracy if it is separated from the boundary of the sensing area more than 2.5 mm.

C. Normal Force Detection Based on I_{all-i} and I_{all-o}

To confirm whether normal force can be estimated from I_{all-i} or I_{all-o}, different normal forces are added at the same points. The loading condition is shown in Fig. 9. The normal force is changed in the range of 0.1 N $\sim$ 4.2 N. Five compression

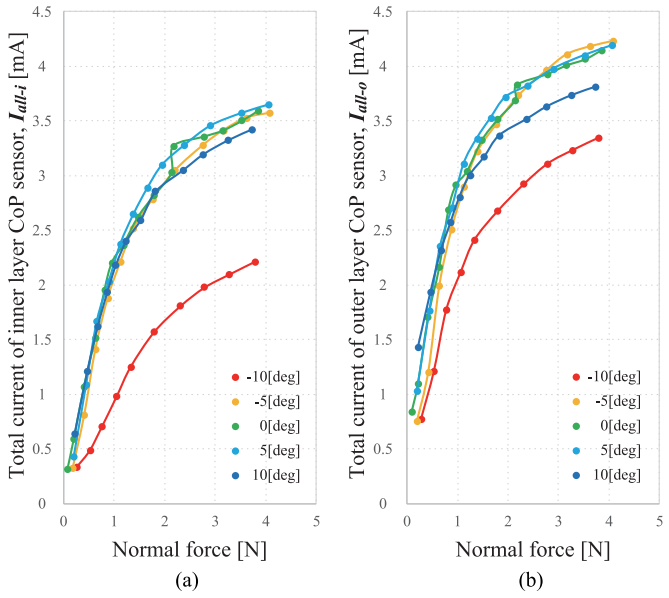

Fig. 10. Experimental result of normal force detection (Relationship between the total current of (a) the inner layer and (b) the outer layer CoP sensors I_{all-i} and the normal force).

points (-10 deg, -5 deg, 0 deg, $+5$ deg, $+10$ deg) are selected to check the difference of the characteristics according to the contact position.

Fig. 10 shows the reaction of (a) I_{all-i} and (b) I_{all-o} to the compressed normal force. It can be seen that, the characteristics of all compression points are almost the same if omitting the data at the compression point of -10 deg. The difference at -10 deg is thought to be caused by a small bending deformation of the fingertip constrained as a cantilever. The values monotonically increase according to the normal force. The gradient is large when the normal force is less than 1 N. Although it decreases at larger normal force, a significant response is confirmed until 4 N. This is enough for manipulating daily objects (usually within the range of 300 g–500 g). The dispersion among the different compression points is smaller at the inner layer. This tendency is remarkable when the normal force is small. Therefore, it is said that the normal force can be accurately estimated from I_{all-i} in almost all range of the sensing area. In addition, it is better that the estimation of the contact position mentioned above uses the inner layer, $\bar{x}_{c-i}$, because the layer is the more sensitive to the same loading condition.

D. Tangential Force Detection Based on s_x

At first, we confirm the validity of the tangential force detection principle proposed in Section II-A. Tangential force from -0.3 N to $+0.3$ N is applied five times at the center of the sensing area. Fig. 11 shows the relationship between the corrected values $\bar{x}_{c-i}$, $\bar{x}_{c-o}$ and the tangential force. The gradient of $\bar{x}_{c-i}$ is significantly larger than that of $\bar{x}_{c-o}$, which supports the proposed principle. The same tendency can be seen in all five times.

Then, to evaluate s_x quantitatively, tangential force is gradually increased from an initial state where compression is

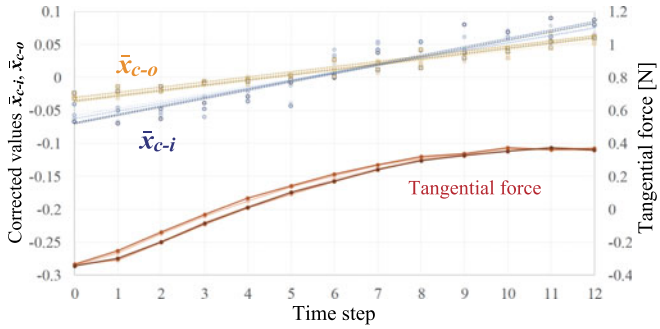

Fig. 11. Result of preliminary experiment to confirm the tangential force estimation principle. (The corrected values $\bar{x}_{c-i}$ and $\bar{x}_{c-o}$ are measured during applying tangential force -0.3 N $\sim +0.3$ N.)

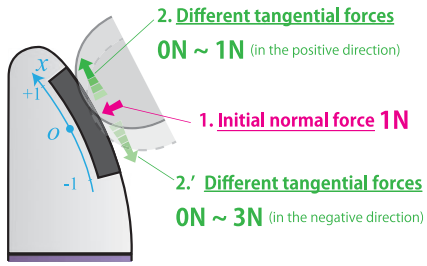

Fig. 12. Loading condition of the experiment of tangential force detection.

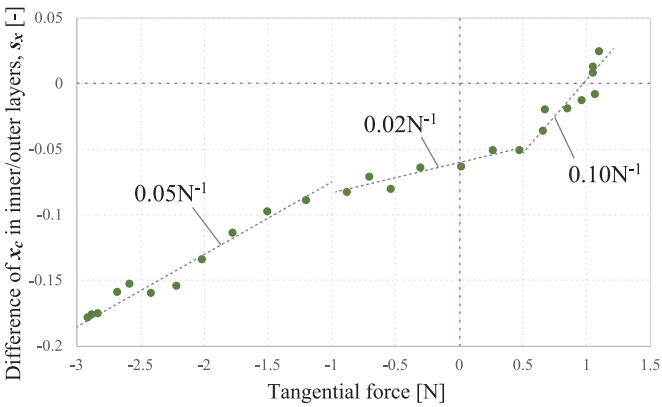

Fig. 13. Experimental result of tangential force detection. (Relationship between the difference of x_c in inner/outer layers s_x and the tangential force.)

executed in normal direction at a point. The loading condition is shown in Fig. 12. The compression point is the center of the sensor (rotational angle is 0 deg). Firstly the indenter is compressed at 1 N in the normal direction, and then, it is gradually moved in both directions along the tangential line. The tangential force is changed in the range of -3 N $\sim +1$ N, where the positive direction is the tip-side of the finger. The range is not beyond the elastic restoring force of the sensor.

Fig. 13 shows the relationship between s_x and the tangential force. Here, s_x is calculated by using the corrected values $\bar{x}_{c-i}$ and $\bar{x}_{c-o}$ (i.e. x_{c-i} and x_{c-o} are replaced by $\bar{x}_{c-i}$ and $\bar{x}_{c-o}$ in the (3)). s_x is positively correlated with the tangential force in all measured range. This means that the tangential force can be estimated from s_x. The rates of change with respect to the tangential force are about 0.05 N^{-1} at -3 N ~ -1 N, 0.02 N^{-}1 at -1 N $\sim +0.5$ N and 0.10 N^{-1} at $+0.5$ N $\sim +1$ N, respectively.

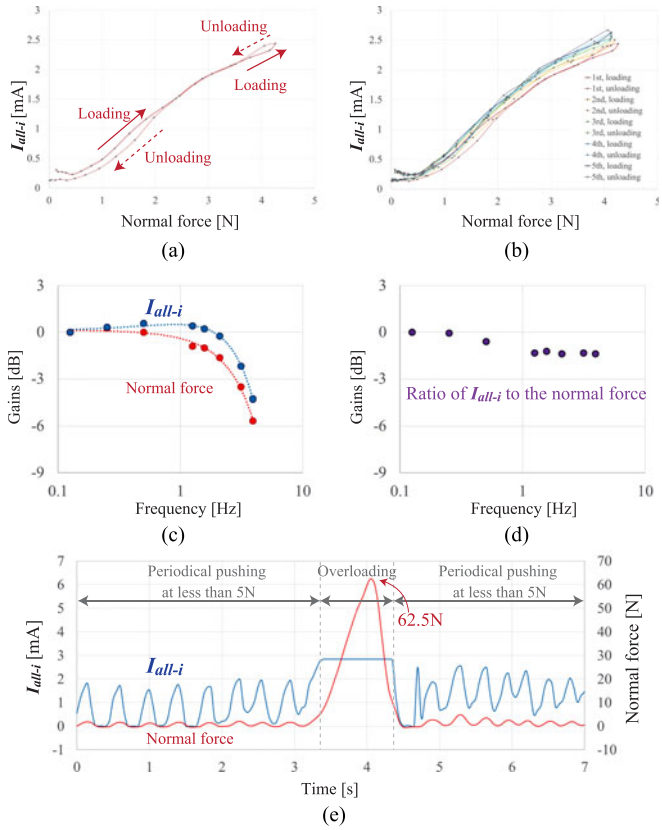

Fig. 14. Experimental results for investigating the specifications: (a) hysteresis, (b) repeatability, (c) (d) responsiveness, and (e) durability.

The sensitivity is not so large, and so the estimation is sensitive to the correction error of x_{c-i} and x_{c-o}. Thus, it is important to minimize the fabrication error of the sensor and to calibrate the sensor outputs.

E. Hysteresis, Repeatability, Responsiveness and Durability

Other specifications of the proposed sensor are verified. Firstly, the hysteresis and the repeatability are investigated by dynamically loading and unloading normal force to the sensor. The indenter is pushed to the position where the normal force is about 4 N at 1.25 mm/s, and then immediately pulled at the same speed. The motion is repeated five times. Fig. 14(a) shows the response of I_{all-i} during the first loading and unloading process. The output values in the processes are sectionally different; the value in unloading is larger in the range of the normal force of 3.5 N or more, and that in loading is larger when the normal force is 2.4 N or less. These are considered to be the influences of viscoelasticity and adsorptive property of the flexible material, respectively. In total, the hysteresis causes difference of I_{all-i} up to 20%, but it is not a critical problem. Fig. 14(b) shows the response during all of the five times. The values are almost the same and so the repeatability is high.

Then, the responsiveness is investigated by applying periodical normal force to the sensor. From the same initial contact state, forced displacements of a triangular waves with the amplitude of 1 mm and the frequency of 0.125 $\sim$ 3.9 Hz are applied

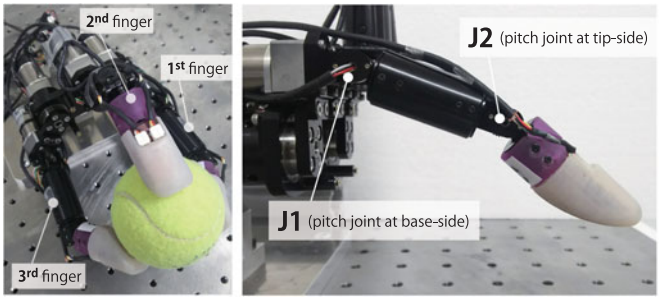

Fig. 15. Robotic hand used in the motion experiments ((a) arrangement of the first, second and third fingers, (b) arrangement of the pitch joints J1 and J2).

to the indenter. Fig. 14(c) shows the response of I_{all-i} and the actual normal force, which are normalized by the values at the minimum frequency (0.125 Hz). The gains begin to decrease at 2 Hz. It suggests that the normal force becomes to less-transmitted at high frequency due to the viscoelasticity of the structure of the fingertip, and so the sensor output is reduced accordingly. When evaluated by the ratio of I_{all-i} to the normal force, as shown in Fig. 14(d), no extreme gain reduction occurs, and it is around -1.4 dB at 3.9 Hz.

Finally, the durability is checked. Using a force sensor (USL06-H5-100N-C, measuring range XY: ± 50 N and Z: $+100$ N, Tec Gihan Co., Ltd.), we investigate the response of I_{all-i} to the normal force when manually applying loading/unloading including large normal force. Fig. 14(e) shows the result. At the time around 4 s, normal force up to 62.5 N acts, and I_{all-i} is saturated. However, immediately after that, the sensor correctly responds to the load which is in the measurement range of the sensor. It is said that the sensor has enough durability to withstand the normal force of 60 N, which greatly exceeds the measurement range.

IV. Feedback Control Laws and Motion Experiments

This section proposes two kinds of feedback control laws of robot fingertips based on force sensing with the fingertip sensor. One is a combination of fundamental feedback controls based on I_{all-i} and $\bar{x}_{c-i}$. It enables to keep both a contact position on the fingertip and normal force at constant when the fingertip touches a movable object. The other is a combination of fundamental feedback controls based on I_{all-i} and s_x. It contributes to keep rolling contact by controlling the fingertip in a contact state where the normal force is constant and the tangential force is zero, respectively. These control laws are validated through motion experiments using an actual robotic hand.

A. Robotic Hand System

The robotic hand used in this letter has three fingers with 8 DOF, produced by Harmonic Drive Systems Inc. (see Fig. 15(a)). Each finger has two pitch joints, and the first and third fingers have roll joints at the bases. Torque control is adopted to all of the joints by using servo drivers (SVEM2 and SVEM4, Servoland corp.). A real-time controller (dSPACE, processor board DS1006, counter board DS3002, DA board DS2103 and AD board DS2002) is applied for sending

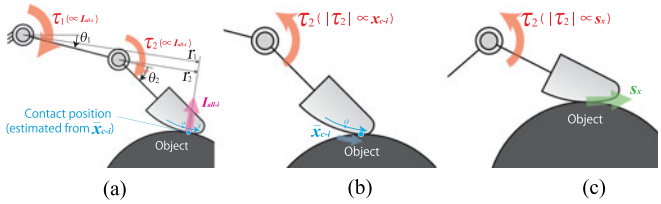

Fig. 16. Fundamental feedback controls based on the proposed sensor (a) for keeping constant normal force to an object, (b) for keeping a contact position at the center of the fingertip, and (c) for keeping rolling contact between the fingertip and the object.

commands to the servo drivers and receiving the outputs from the fingertip sensors. The output cables can be directly connected to the AD board, without requiring additional electronics. Both of the sampling rate of the sensor output and the control frequency of the robotic hand are 10 kHz. In the experiments, we use the two pitch joints of the third finger (Fig. 15(b)). Here, the base-side joint is called J1, and the tip-side joint is J2.

B. Feedback Control Law Based on I_{all-i} and $\bar{x}_{c-i}$

Fig. 16(a) and (b) explain the two fundamental feedback controls based on I_{all-i} and $\bar{x}_{c-i}$. The control in Fig. 16(a) is for keeping constant normal force. The contact position on the fingertip can be estimated from $\bar{x}_{c-i}$, and the normal force acting on the position can be estimated from I_{all-i}. Thus, $I_{all-ref}$, a target value of I_{all-i}, is initially determined according to the target normal force. Then, the torques on J1 and J2 are generated in proportion to the deviation $I_{all-ref} - I_{all-i}$ with considering the moment arms r_1 and r_2 from the joints to the contact position. On the other hand, the control in Fig. 16(b) is for keeping the contact position at the center of the fingertip, where the target value of $\bar{x}_{c-i} = 0$. The torque on J2 is generated in proportion to $-\bar{x}_{c-i}$.

Thus, τ_1 and τ_2, the input torques of J1 and J2, are given by the following equations,

$$\tau_1 = k_n(I_{all-ref} - I_{all-i}), \tag{6}$$

$$\tau_2 = k_n \frac{r_2}{r_1}(I_{all-ref} - I_{all-i}) - k_p \bar{x}_{c-i} \tag{7}$$

Here, k_n and k_p are constant gains.

Fig. 17 shows snapshots and measured data of the motion experiment. Here, the parameters are set as $I_{all-ref} = 1$ mA, $k_n = 0.25$, and $k_p = 0.3$, and the object to be touched is a human finger. Fig. 17(a) is the data in the time range of $t = 2.5 \sim 4.5$ s, where the object is statically held to the robot finger. It can be seen that $\bar{x}_{c-i}$ converges at zero in short time and I_{all-i} gradually becomes close to $I_{all-ref}$. Note that steady-state deviation remains in I_{all-i} because the control law applies only proportional members for simplicity. According to the sensor outputs, τ_1 gradually decreases, and τ_2 decreases at first for the feedback of $\bar{x}_{c-i}$ and then increases. Both θ_1 and θ_2, the joint angles of J1 and J2, keep constant values. In the time range of $t = 5 \sim 7$ s (Fig. 17(b)), the object is periodically pushed to the robot finger. It can be seen that τ_1 and τ_2 change in synchronization with increase/decrease of I_{all-i}, Following this, $\bar{x}_{c-i}$ increases/decreases with a slight delay, which brings a change

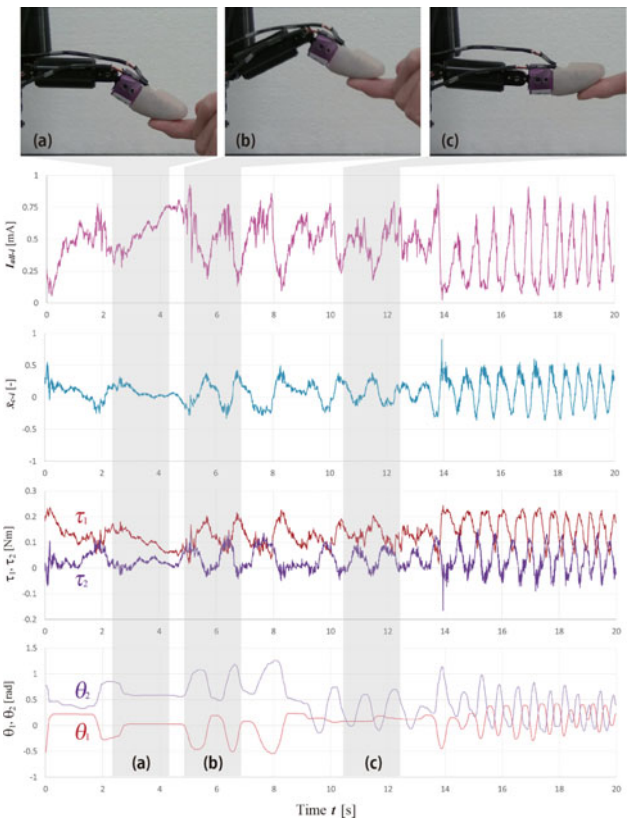

Fig. 17. Experimental result of the feedback control law based on I_{all-i} and $\bar{x}_{c-i}$. (Snapshots of three scenes and measured data of I_{all-i}, $\bar{x}_{c-i}$, τ_1, τ_2, θ_1 and θ_2 are shown. In the time range (a) ($t = 2.5 \sim 4.5$ s), the object is statically held to the robot finger. In the time range (b) ($t = 5 \sim 7$ s), the object is periodically pushed to the robot finger. In the time range (c) ($t = 10.5 \sim 12.5$ s), the object is moved along the robot finger surface.)

of τ_2. As the result, θ_1 and θ_2 move positively and negatively according to the movement of the object. In the time range of $t = 10.5 \sim 12.5$ s (Fig. 17(c)), the object is moved along the robot finger surface. Focusing on the movement from $t = 11$ s, increase of $\bar{x}_{c-i}$ and decrease of τ_2 appear in advance. It brings decrease of I_{all-i}, and so τ_1 and τ_2 increases responsively. As the result, only the movement of θ_2 is observed.

Therefore, it is confirmed that the combination of the fundamental feedback controls based on I_{all-i} and $\bar{x}_{c-i}$ enables the robotic finger to keep the contact position and the normal force constant to the object.

C. Feedback Control Law Based on I_{all-i} and s_x

Next, the two fundamental feedback controls based on I_{all-i} and s_x are explained. Here, the control in Fig. 16(c), which is for rotating the fingertip along the object surface to the direction opposite to the tangential force, is applied instead of that in Fig. 16(b). The rotation of the fingertip is produced by generating the torque on J2 in proportion to $-s_x$. In this case, τ_1 and τ_2 are given as follows,

$$\tau_1 = k_n(I_{all-ref} - I_{all-i}), \tag{8}$$

$$\tau_2 = k_n \frac{r_2}{r_1}(I_{all-ref} - I_{all-i}) - k_t s_x \tag{9}$$

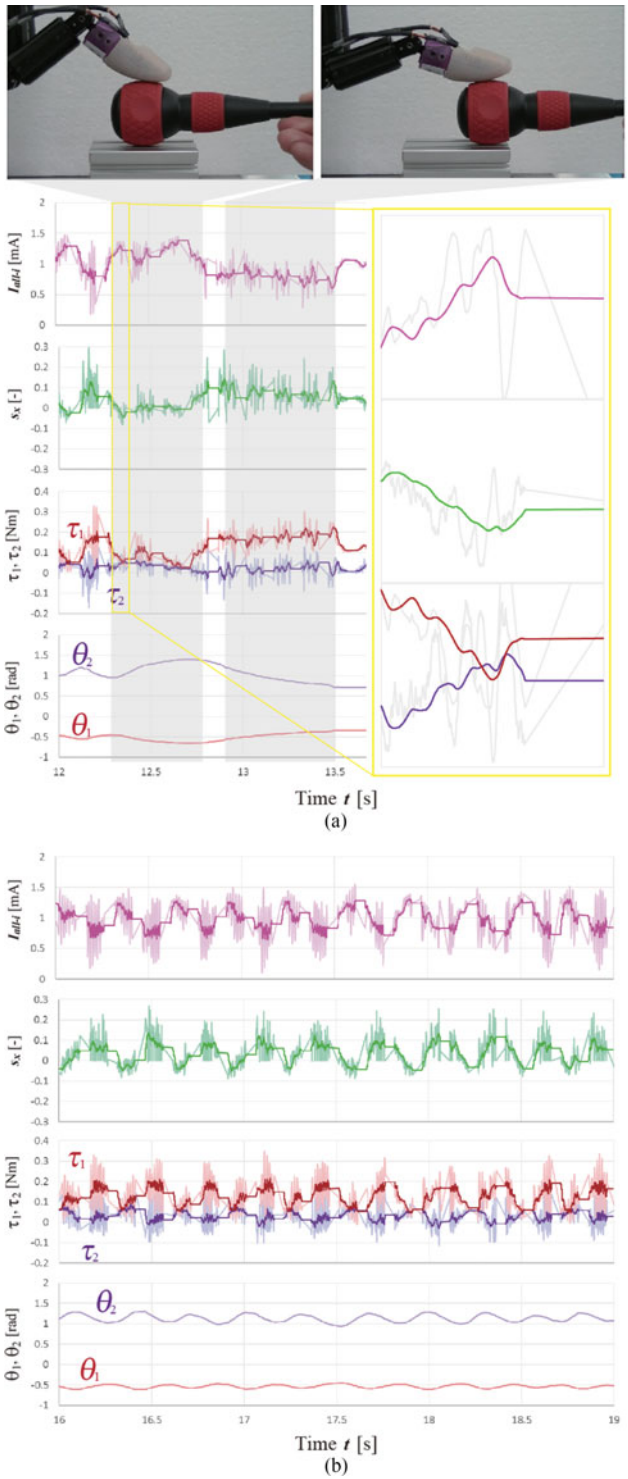

Fig. 18. Experimental result of the feedback control law based on I_{all-i} and s_x ((a) snapshots and measured data of I_{all-i}, s_x, τ_1, τ_2, θ_1 and θ_2 during the object is pushed and pulled to the robotic hand, (b) Those during the object is periodically pushed and pulled in approximately 3 Hz).

Here, k_t is a constant gain.

In the motion experiment, the parameters are set as $I_{all-ref} = 1.5$ mA, $k_n = 0.25$, and $k_t = 0.8$, and a grip section of a screwdriver is chosen as the target object because of its suitable size, hardness and friction. The reason why $I_{all-ref}$ is larger than that

in the first experiment is because it was observed, in a preliminary experiment, that s_x was sensitive to tangential force when normal force was large. In addition, divergence of s_x rarely occurred because of unstable $\bar{x}_{c-o}$ when I_{all-o} was small. Thus, the following conditional equation is applied in this experiment by setting a threshold as $I_{all-th} = 0.3$ mA.

$$s_x = \begin{cases} 0 & (I_{all-o} < I_{all-th}) \\ \bar{x}_{c-i} - \bar{x}_{c-o} & (I_{all-o} \geq I_{all-th}). \end{cases} \tag{10}$$

Fig. 18 shows snapshots and measured data in two time ranges in the experiment. There is a small amplitude and high frequent oscillation of the robot finger, which is thought to be caused by the large $I_{all-ref}$. To see the tendencies of I_{all-i}, s_c, τ_1 and τ_2, 20 ms moving averages are added in the graphs.

The two highlighted areas in Fig. 18(a) correspond to time sections when the object is pushed and pulled against the robotic hand, respectively. Comparing the two snapshots, we can see that the contact position on the fingertip changes adaptively; at the tip-side in the pushed section, and at the base-side in the pulled section. In the pushed section, s_x decreases because tangential force occurs in the negative direction, which brings increase of τ_2. This torque temporarily makes I_{all-i} become larger, which then brings decrease of both τ_1 and τ_2. As the result, J1 moves outward and J2 moves inward as shown in the graphs of θ_1 and θ_2, and so the contact position is translated to the tip-side. In the same manner, the opposite movement in the pulled section can be explained. Fig. 18(b) shows the data when the object is periodically pushed and pulled in approximately 3 Hz. We can see that the adaptive rotation of the robot fingertip mentioned above is applicable to such a quick motion of the object.

Therefore, it is confirmed that the combination of fundamental feedback controls based on I_{all-i} and s_x enables the robotic finger to keep rolling contact to the object.

V. Conclusion

This letter proposed a sheet-shaped force sensor for a robot fingertip. One of the important advantages is that the sensor can be designed adaptively to various shapes of fingertips. Thus, the method would be applicable to other robotic hands, robot arms, torso and other types of robots. The contact position can be estimated in high accuracy in almost all of the sensing area. The normal force can be estimated independent with the contact position. The tangential force can be also estimated, but the sensitivity remains to be improved. In addition, this letter presented feedback control laws of a robot finger mounted with the proposed sensor. The combination of fundamental feedback controls based on estimated values of the normal force and the contact position enabled the robotic finger to keep the contact position and the normal force constant to the object. The combination of fundamental feedback controls based on estimated values of the normal and tangential forces enabled the robotic finger to keep rolling contact to the object.

Our future works are improvement of the sensor and application to manipulation tasks. The sensing area should be enlarged to fulfill the fingertip surface, or whole surface of the robotic hand. The sensor structure would be modified to detect 2-D tangential force by using 2-D CoP sensors. These improvements are helpful for realizing manipulation tasks such as grasping a moving object and managing human tools.

References

[1] D. E. Whitney, "Quasi-static assembly of compliantly supported rigid parts," *J. Dyn. Sys. Meas., Control*, vol. 104, no. 1, pp. 65–77, 1982.

[2] G. Figliolini and M. Ceccarelli, "A novel articulated mechanism mimicking the motion of index fingers," *Robotica*, vol. 20, no. 1, pp. 13–22, 2002.

[3] L. U. Odhner *et al.*, "A compliant, underactuated hand for robust manipulation," *Int. J. Robot. Res.*, vol. 33, no. 5, pp. 736–752, 2014.

[4] E. Farnioli, M. Gabiccini, M. Bonilla, and A. Bicchi, "Grasp compliance regulation in synergistically controlled robotic hands with VSA," in *Proc. 2013 IEEE/RSJ Int. Conf. Intell. Robots Syst.*, 2013, pp. 3015–3022.

[5] A. M. Dollar and R. D. Howe, "The highly adaptive SDM hand: Design and performance evaluation," *Int. J. Robot. Res.*, vol. 29, no. 5, pp. 585–597, 2010.

[6] E. Brown *et al.*, "Universal robotic gripper based on the jamming of granular material," *Proc. Nat. Acad. Sci. USA*, vol. 107, no. 44, pp. 18809–18814, 2010.

[7] J. R. Amend, E. Brown, N. Rodenberg, H. M. Jaeger, and H. Lipson, "A positive pressure universal gripper based on the jamming of granular material," *IEEE Trans. Robot.*, vol. 28, no. 2, pp. 341–350, Apr. 2012.

[8] T. Nishimura, Y. Fujihira, R. Adachi, and T. Watanabe, "New condition for tofu stable grasping with fluid fingertips," *Proc. 2016 IEEE Int. Conf. Autom. Sci. Eng.*, 2016, pp. 335–341.

[9] J. A. Maples and J. J. Becker, "Experiments in force control of robotic manipulators," *Proc. 1986 IEEE Int. Conf. Robot. Autom.*, 1986, pp. 695–702.

[10] M. R. Cutkosky and I. Kao, "Computing and controlling the compliance of a robotic hand," *IEEE Trans. Robot. Autom.*, vol. 5, no. 2, pp. 151–165, Apr. 1989.

[11] M. H. Raibert and J. J. Craig, "Hybrid position/force control of manipulators," *Trans. ASME*, vol. 102, pp. 126–133, 1981.

[12] T. Murakami, R. Nakamura, F. Yu, and K. Ohnishi, "Force sensorless impedance control by disturbance observer," in *Proc. Conf. Rec. Power Convers. Conf.*, 1993, pp. 352–357.

[13] A. D. Luca and R. Mattone, "Sensorless robot collision detection and hybrid force/motion control," in *Proc. 2005 IEEE Int. Conf. Robot. Autom.*, 2005, pp. 999–1004.

[14] M. P. Polverini, A. M. Zanchettin, S. Castello, and Paolo Rocco, "Sensorless and constraint based peg-in-hole task execution with a dual-arm robot," in *Proc. 2016 IEEE Int. Conf. Robot. Autom.*, 2016, pp. 415–420.

[15] R. S. Dahiya, P. Mittendorfer, M. Valle, G. Cheng, and V. J. Lumelsky, "Directions toward effective utilization of tactile Skin: A review," *IEEE Sensors J.*, vol. 13, no. 11, pp. 4121–4138, Nov. 2013.

[16] M. Ishikawa and M. Shimojo, "A method for measuring the center position of a two dimensional distributed load using pressure-conductive rubber," *Trans. Soc. Instrum. Control Engineers*, vol. 18, no. 7, pp. 730–735, 1982.

[17] M. Shimojo, T. Araki, S. Teshigawara, A. Ming, and M. Ishikawa, "A net-structure tactile sensor covering free-form surface and ensuring high-speed response," in *Proc. 2007 IEEE/RSJ Int. Conf. Intell. Robots Syst.*, 2007, pp. 670–675.

[18] SynTouch. [Online]. Available: https://www.syntouchinc.com/sensor-technology/, Accessed on: Feb. 15, 2017.

[19] C. G. Núñez, W. T. Navaraj, E. O. Polat, and R. Dahiya, "Energy-autonomous, flexible, and transparent tactile skin," *Adv. Functional Mater.*, vol. 27, no. 18, 2017.

[20] OptoForce. [Online]. Available: http://optoforce.com/, Accessed on: Feb. 15, 2017.

[21] D. M. Vogt, Y. L. Park, and R. J. Wood, "Design and characterization of a soft multi-axis force sensor using embedded microfluidic channels," *IEEE Sensors J.*, vol. 13, no. 10, pp. 4056–4064, Oct. 2013.

[22] T. P. Tomo *et al.*, "A modular, distributed, soft, 3-axis sensor system for robot hands," *Proc. 216 IEEE-RAS 16th Int. Conf. Humanoid Robots*, 2016, pp. 454–460.

[23] P. Yu, W. Liu, C. Gu, X. Cheng, and X. Fu, "Flexible piezoelectric tactile sensor array for dynamic three-axis force measurement," *Sensors*, vol. 16, no. 6, p. 819, 2016.